HERAFitter

Open Source QCD Fit Project

Version 0.91 (svn 1468)

```
S. Alekhin<sup>16,17</sup>, O. Behnke<sup>1</sup>, P. Belov<sup>1,12</sup>, M. Botje<sup>18</sup>, D. Britzger<sup>1</sup>, S. Camarda<sup>1</sup>,
A.M. Cooper-Sarkar<sup>2</sup>, K. Daum<sup>30,31</sup>, C. Diaconu<sup>3</sup>, J. Feltesse<sup>19</sup>, A. Gizhko<sup>1</sup>,
A. Glazov<sup>1</sup>, A. Guffanti<sup>20</sup>, M. Guzzi<sup>1</sup>, F. Hautmann<sup>13,14,15</sup>, A. Jung<sup>32</sup>, H. Jung<sup>1,33</sup>
V. Kolesnikov<sup>4</sup>, H. Kowalski<sup>1</sup>, O. Kuprash<sup>1</sup>, A. Kusina<sup>21</sup>, S. Levonian<sup>1</sup>, K. Lipka<sup>1</sup>,
B. Lobodzinski<sup>29</sup>, K. Lohwasser<sup>16</sup>, A. Luszczak<sup>5</sup>, B. Malaescu<sup>25</sup>, R. McNulty<sup>28</sup>,
V. Myronenko<sup>1</sup>, S. Naumann-Emme<sup>1</sup>, K. Nowak<sup>1</sup>, F. Olness<sup>21</sup>, E. Perez<sup>23</sup>, H. Pirumov<sup>1</sup>,
R. Plačakytė<sup>1</sup>, K. Rabbertz<sup>6</sup>, V. Radescu<sup>1</sup>, R. Sadykov<sup>24</sup>, G. Salam<sup>26,27</sup>, A. Sapronov<sup>4</sup>,
A. Schöning<sup>10</sup>, T. Schörner-Sadenius<sup>1</sup>, S. Shushkevich<sup>1</sup>, W. Slominski<sup>7</sup>, H. Spiesberger<sup>22</sup>,
P. Starovoitov<sup>1</sup>, M. Sutton<sup>8</sup>, J. Tomaszewska<sup>9</sup>, O. Turkot<sup>1</sup>, A. Vargas<sup>1</sup>, G. Watt<sup>11</sup>,
K. Wichmann<sup>1</sup>
<sup>1</sup>Deutsches Elektronen-Synchrotron (DESY), Hamburg, Germany
<sup>2</sup> Department of Physics, University of Oxford, Oxford, United Kingdom
<sup>3</sup> CPPM, IN2P3-CNRS, Univ. Mediterranee, Marseille, France
<sup>4</sup> Joint Institute for Nuclear Research (JINR), Joliot-Curie 6, 141980, Dubna, Moscow Region, Russia
<sup>5</sup> T. Kosciuszko Cracow University of Technology
<sup>6</sup> Institut für Experimentelle Kernphysik, Karlsruhe, Germany
<sup>7</sup> Jagiellonian University, Institute of Physics, Ul. Reymonta 4, PL-30-059 Cracow, Poland
<sup>8</sup> University of Sussex, Department of Physics and Astronomy, Sussex House, Brighton BN1 9RH, United Kingdom
<sup>9</sup> Warsaw University of Technology, Faculty of Physics, Koszykowa 75, 00-662 Warsaw, Poland
<sup>10</sup> Physikalisches Institut, Universität Heidelberg, Heidelberg, Germany
<sup>11</sup> Institute for Particle Physics Phenomenology, Durham University, Durham, DH1 3LE, United Kingdom
<sup>12</sup> Current address: Department of Physics, St. Petersburg State University, Ulyanovskaya 1, 198504 St. Petersburg, Russia
<sup>13</sup> Dept. of Physics and Astronomy, University of Sussex, Brighton BN1 9QH, United Kingdom
<sup>14</sup> Rutherford Appleton Laboratory, Chilton OX11 0QX, United Kingdom
<sup>15</sup> Dept. of Theoretical Physics, University of Oxford, Oxford OX1 3NP, United Kingdom
<sup>16</sup> Deutsches Elektronen-Synchrotron (DESY), Platanenallee 6, D15738 Zeuthen, Germany
<sup>17</sup> Institute for High Energy Physics,142281 Protvino, Moscow region, Russia
<sup>18</sup> Nikhef, Science Park, Amsterdam, the Netherlands
<sup>19</sup> CEA, DSM/Irfu, CE-Saclay, Gif-sur-Yvette, France
<sup>20</sup> Niels Bohr Institute, University of Copenhagen, Denmark
<sup>21</sup> Southern Methodist University, Dallas, Texas
<sup>22</sup> PRISMA Cluster of Excellence, Institut für Physik (WA THEP), Johannes-Gutenberg-Universität, D-55099 Mainz, Germany
<sup>23</sup> CERN, European Organization for Nuclear Research, Geneva, Switzerland
<sup>24</sup> Joint Institute for Nuclear Research, Joliot-Curie str. 6, Dubna, 141980, Russia
<sup>25</sup> Laboratoire de Physique Nucléaire et de Hautes Energies, UPMC and Université, Paris-Diderot and CNRS/IN2P3, Paris, France
<sup>26</sup> CERN, PH-TH, CH-1211 Geneva 23, Switzerland
<sup>27</sup> LPTHE; CNRS UMR 7589; UPMC Univ. Paris 6; Paris 75252, France
<sup>28</sup> University College Dublin, Dublin 4, Ireland
<sup>29</sup> Max Planck Institut Für Physik, Werner Heisenberg Institut, Föhringer Ring 6, Munchen
30 Fachbereich C, Universität Wuppertal, Wuppertal, Germany
<sup>31</sup> Rechenzentrum, Universität Wuppertal, Wuppertal, Germany
32 FERMILAB, Batavia, IL, 60510, USA
<sup>33</sup> Elementaire Deeltjes Fysica, Universiteit Antwerpen, B 2020 Antwerpen, Belgium
Received: date / Accepted: date
```

Abstract HERAFitter [1] is an open-source package which provides a framework for the determination of the parton distribution functions (PDFs) of the proton and for multifold analyses in Quantum Chromodynamics (QCD).

Measurements of lepton-proton deep inelastic scattering (DIS) and of proton-proton (proton-antiproton) collisions at hadron colliders are included in the HERAFitter package, analyses in Quantum Chromodynamics (QCD).

8 and are used to probe and constrain the partonic content of

The partonic distributions are determined by using the factorisation properties of the hadronic cross sections in which short-distance perturbatively calculable hard scatterings and long-distance contributions that are the non-perturbative universal PDFs, are factorised.

The HERAFitter platform provides a broad choice of options for the treatment of the experimental uncertainties and a common environment where a large number of theoretical calculations and methodological options are used to perform detailed QCD analyses. The general structure of HERAFitter together with available methods are described in this paper.

22 Keywords PDFs · QCD · Fit · proton structure

Contents

Introduction

-	•	III	addion	_			
5	2	HERAFitter Structure					
6	3	Theoretical Input					
7		3.1	Deep Inelastic Scattering and Proton Sructure	4			
18		3.2	Electroweak Corrections to DIS	5			
19		3.3	Diffractive PDFs	6			
0		3.4	Drell-Yan processes in pp or $p\bar{p}$ collisions	6			
1		3.5	Jet production in ep and pp or $p\bar{p}$ collisions	6			
2		3.6	Top-quark production in pp and $p\bar{p}$ collisions	7			
3 4	4	Com	putational Techniques	7			
4		4.1	<i>k</i> -factor Technique	7			
5		4.2	Fast Grid Techniques	7			
6	5	Fit Methodology					
7		5.1	Functional Forms for PDF parametrisation	8			
8		5.2	Representation of χ^2	10			
9		5.3	Treatment of the Experimental Uncertainties	10			
-0		5.4	Treatment of the Theoretical Input Parameters	11			
1		5.5	Bayesian Reweighting Techniques	11			
2	6	Alternatives to DGLAP formalism					
3		6.1	DIPOLE models	12			
4		6.2	Transverse Momentum Dependent (Unintegrated) PDFs				
5			with CCFM	12			
6	7	Applications of HERAFitter					
7	8	Summary					

48 1 Introduction

unprecedented accuracy from hadron colliders is a remark- 888 comparisons of different theoretical approaches and can be able challenge for the high energy physics community to 89 used for direct tests of the impact of new experimental data provide higher-order theory predictions and to develop effi- 90 in the QCD analyses. cient tools and methods for data analysis. The recent discovery of the Higgs boson [2, 3] and the extensive searches for 92 overview of HERAFitter is presented in section 2. Section 3 signals of new physics in LHC proton-proton collisions de- 93 discusses the various processes and corresponding theoretmand high-precision computations to test the validity of the 94 ical calculations performed in the DGLAP [6–10] formal-Standard Model (SM) and factorisation in Quantum Chro- 95 ism, available in HERAFitter. Section 4 presents various modynamics (QCD). According to collinear factorisation in 96 fast techniques employed by the theory calculations used in

perturbative QCD (pQCD) hadronic inclusive cross sections are written as

$$\sigma(\alpha_{s}, \mu_{R}, \mu_{F}) = \sum_{a,b} \int_{0}^{1} dx_{1} dx_{2} f_{a}(x_{1}, \alpha_{s}, \mu_{F}) f_{b}(x_{2}, \alpha_{s}, \mu_{F})
\times \hat{\sigma}^{ab}(x_{1}, x_{2}; \alpha_{s}, \mu_{R}, \mu_{F}),$$
(1)

where the cross section σ for any hard-scattering inclusive process is expressed as a convolution of Parton Distribution Functions (PDFs) f_a and f_b with the partonic cross section $\hat{\sigma}^{ab}$. The PDFs represent the probability of finding a specific parton a(b) in the first (second) proton carrying a fraction x_1 $_{54}$ (x_2) of its momentum. Indices a and b in the Eq. 1 indicate 55 the various kinds of partons, i.e. gluons, quarks and antiquarks of different flavours, that are considered as the constituents of the proton. Both the PDFs and the partonic cross section depend on the strong coupling α_s , and the factorisation and renormalisation scales, μ_F and μ_R , respectively. The partonic cross sections $\hat{\sigma}^{ab}$ are calculated in pQCD whereas PDFs are constrained by global fits to variety of the hardprocess experimental data employing universality of PDFs within a particular factorization scheme [4, 5].

Measurements of the inclusive Neutral Current (NC) and Charged Current (CC) Deep-Inelastic-Scattering (DIS) at the ep collider HERA provide crucial information for determin- $_{67}$ ing the PDFs. The gluon density in small and medium x68 can be accurately determined solely from the HERA data. Many processes in pp and $p\bar{p}$ collisions at LHC and Teva-⁷⁰ tron, respectively, probe PDFs in the kinematic ranges, complementary to the DIS measurements. Therefore inclusion 72 of the LHC and Tevatron data in the QCD analysis of the 73 proton structure provide additional constraints on the PDFs, 74 improving either their precision, or providing valuable in-75 formation on the correlations of PDF with the fundamental 76 QCD parameters like strong coupling or quark masses. In 77 this context, the processes of interest at hadron colliders are 78 Drell-Yan (DY) production, W-boson asymmetries, associ-79 ated production of W or Z bosons and heavy quarks, top 80 quark, jet and prompt photon production.

The open-source QCD platform HERAFitter encloses 82 the set of tools necessary for a comprehensive global OCD analysis of hadron-induced processes even at the early stage of the experimental measurement. It has been developed for 85 determination of PDFs and extraction of fundamental QCD 86 parameters such as the heavy quark masses or the strong The constant inflow of new experimental measurements with 87 coupling constant. This platform also provides the basis for

This paper is organised as follows. The structure and

HERAFitter. Section 5 elucidates the methodology of determining PDFs through fits based on various χ^2 definitions used in the minimisation procedure. Alternative approaches to the DGLAP formalism are presented in section 6. Specific applications of the package are given in section 7 and the summary is presented in section 8.

2 HERAFitter Structure

HERAFitter is a flexible open-source platform for the QCD analyses of different experimental measurements, providing a versatile environment for benchmarking studies. It is widely used within LHC experiments [11–17].

The functionality of HERAFitter is schematically illustrated in Fig. 1 and it can be divided in four main blocks:

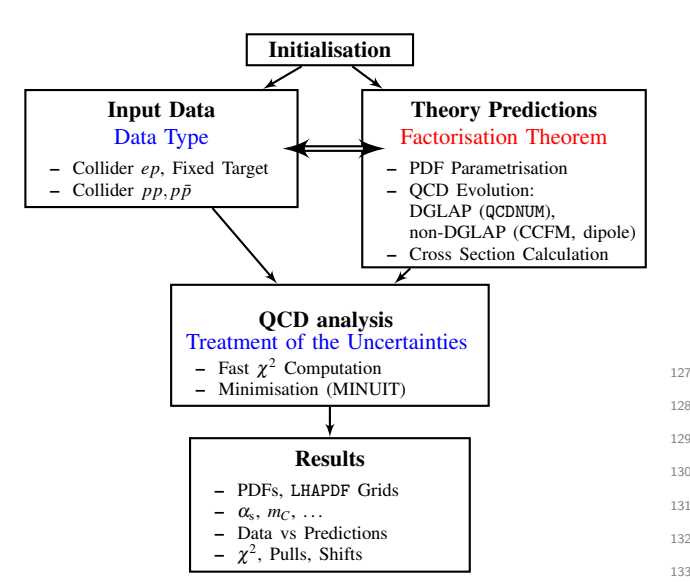


Fig. 1 Schematic structure of the HERAFitter program.

110

114

115

116

118

119

120

124

125

126

Input data: Different available measurements from the var- 137 ious processes are implemented in the HERAFitter pack-138 age including the full information on their uncorrelated 139 and correlated uncertainties. HERA data are sensitive to 140 light quark and gluon densities mostly through scaling 141 violations, covering low and medium x ranges. These 142 data are the basis of any proton PDF extraction, and 143 are used by all global PDF groups [18-22]. However, 144 improvements in precision of PDFs require additional 145 constraints on the gluon and quark distributions at high- 146 x, better understanding of heavy quark distributions and 147 decomposition of the light-quark sea. For these purposes, 148 the measurements of the fixed-target experiments, Teva- 149 tron and LHC are of particular importance. The pro- 150 cesses that are currently available in HERAFitter frame- 151 work are listed in Tab. 1.

Data	Process	Reaction	Theory calculations, schemes
HERA	DIS NC	$ep \rightarrow eX$	TR', ACOT ZM (QCDNUM) FFN (DPENQCDRAD, QCDNUM), TMD (uPDFevolv)
	DIS CC	$ep ightarrow v_e X$	ACOT, ZM (QCDNUM) FFN (OPENQCDRAD)
	DIS jets	$ep \rightarrow e$ jets	NLOJet++ (fastNLO)
	DIS heavy quarks	$ep \rightarrow ec\bar{c}X, \\ ep \rightarrow eb\bar{b}X$	ZM (QCDNUM), TR', ACOT, FFN (OPENQCDRAD, QCDNUM)
Fixed Target	DIS NC	$ep \rightarrow eX$	ZM (QCDNUM), TR', ACOT, FFN (OPENQCDRAD, QCDNUM)
Tevatron, LHC	Drell-Yan	$pp(\bar{p}) \rightarrow l\bar{l}X, \ pp(\bar{p}) \rightarrow l\nu X$	MCFM (APPLGRID)
	top pair	$pp(\bar{p}) \rightarrow t\bar{t}X$	MCFM (APPLGRID), HATHOR
	single top	$ \begin{array}{c c} pp(\bar{p}) \rightarrow tlvX, \\ pp(\bar{p}) \rightarrow tX, \\ pp(\bar{p}) \rightarrow tWX \end{array} $	MCFM (APPLGRID)
	jets	$pp(\bar{p}) \rightarrow \mathrm{jets}X$	NLOJet++ (APPLGRID), NLOJet++ (fastNLO)
LHC	DY+heavy quarks	$pp \rightarrow VhX$	MCFM (APPLGRID)

Table 1 The list of processes available in the HERAFitter package. The references for the individual calculations and their implementations are given in the text.

Theory predictions: Predictions for cross section of different processes are obtained using the factorisation approach (Eq. 1). The PDFs are parametrised at a starting input scale Q_0^2 by a chosen functional form with a set of free parameters **p**. These PDFs are evolved to the scale of the measurement Q^2 , $Q^2 > Q_0^2$. The evolution follows either DGLAP [6–10] (as implemented in QCDNUM [23]), CCFM [24–27] or dipole models [28–30]. The prediction of a particular process cross section is obtained by a convolution of the evolved PDFs and the partonic cross section, calculated at a certain order in QCD with a relevant theory program (as listed in Tab. 1).

134

135

136

QCD analysis: The PDFs are are determined by the least square fit, minimising the χ^2 function with respect to **p** using the MINUIT [31] program. Various choices of accounting for the experimental uncertainties are employed in HERAFitter, either using a nuisance parameter method for the correlated systematic uncertainties, or a covariance matrix method as described in section 5.2). In addition, HERAFitter allows to study different statistics assumptions for the distributions of the systematic uncertainties i.e. Gauss [32] (see section 5.3).

Results: The resulting PDFs are provided in a format ready to be used by the LHAPDF library [33, 34] (or by TMDlib [35]). HERAFitter drawing tools can be used to display the PDFs with their uncertainties at a chosen scale. As an

155

156

157

158

160

162

163

164

165

example, a first set of PDFs extracted using HERAFitter 168 3 Theoretical Input from HERA I data, HERAPDF1.0 [36], is shown in Fig. 2.

dictions are also produced. The inclusive NC data from 170 cesses available in HERAFitter is described.

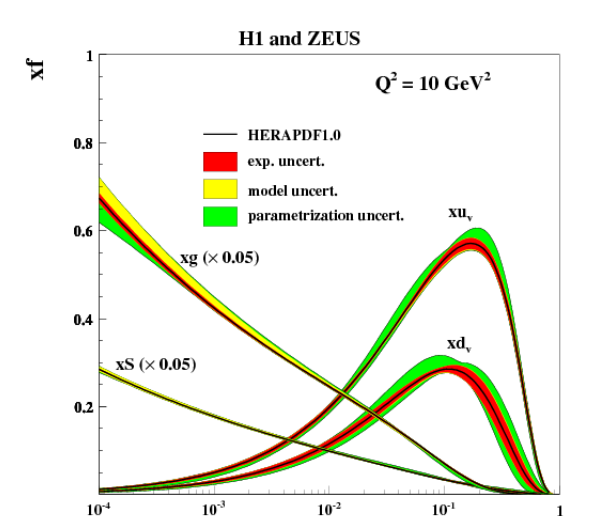


Fig. 2 Distributions of valence (xu_v, xd_v) , sea (xS) and the gluon (g)densities in HERAPDF1.0 [36]. The gluon and the sea distributions are scaled down by a factor of 20. The experimental, model and parametrisation uncertainties are shown as colored bands.

the HERA I are compared with the predictions based on HERAPDF1.0 PDFs in Fig. 3.

Also shown are theory predictions, obtained using the nuisance parameter method, which accounts for correlated systematic shifts when using the nuisance parameter method that accounts for correlated systematic uncertainties. The consistency of the measurements and the theory is expressed by pulls, defined as a difference between data and theory divided by the uncorrelated error of the data. In each kinematic bin of the measurement, pulls are provided in units of sigma.

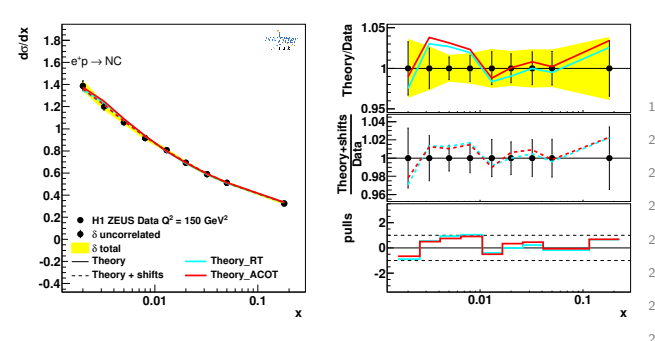


Fig. 3 An illustration of the consistency of HERA measurements [36] and the theory predictions, obtained in HERAFitter with the default drawing tool.

208

209

The comparison of data used in the fit to the theory pre- 169 In this section the theoretical formalism for various pro-

3.1 Deep Inelastic Scattering and Proton Sructure

DIS data provide the backbone of any PDF fit. The formalism that relates the DIS measurements to pQCD and the PDFs has been described in detail in many extensive reviews (see e.g. [37]) and it is only briefly summarised here. DIS is the process where a lepton scatters off the constituents of the proton by a virtual exchange of a NC or CC vector boson and, as a result, a scattered lepton and a multihadronic final state are produced. The common DIS kinematic variables are the absolute squared four-momentum of the exchange boson, Q^2 , the Bjorken x, and the inelasticity y, related by $y = Q^2/sx$, where s is the squared centre-of-mass (c.o.m)

184 The NC cross section can be expressed in terms of generalised structure functions:

$$\frac{d^2 \sigma_{NC}^{e^{\pm} p}}{dx dQ^2} = \frac{2\pi \alpha^2}{x Q^4} \left[Y_+ \tilde{F}_2^{\pm} \mp Y_- x \tilde{F}_3^{\pm} - y^2 \tilde{F}_L^{\pm} \right], \tag{2}$$

where $Y_{\pm} = 1 \pm (1 - y)^2$ (additional terms of $O(1/Q^2)$ are ¹⁸⁷ numerically small at the HERA kinematics are neglected). The generalised structure functions $\tilde{F}_{2,3}$ can be written as linear combinations of the proton structure functions $F_2, F_{2,3}^{\gamma Z}$ and $F_{2,3}^Z$ associated to pure photon exchange terms, photon-Z interference terms and pure Z exchange terms, respectively. 192 Structure function \tilde{F}_2 is the dominant contribution to the cross section, $x\tilde{F}_3$ becomes important at high Q^2 and \tilde{F}_L is 194 sizable only at high y.

The inclusive CC *ep* cross section can be expressed in terms of another set of structure functions and in LO the e^+p and $e^{-}p$ cross sections are sensitive to different combinations of 198 the quark flavour densities:

$$\sigma_{CC}^{e^+p} \approx x[\overline{u} + \overline{c}] + (1 - y)^2 x[d + s],$$

$$\sigma_{CC}^{e^-p} \approx x[u + c] + (1 - y)^2 x[\overline{d} + \overline{s}].$$
(3)

The QCD predictions for the DIS structure functions are obtained by convoluting the PDFs with the respective coefficient functions. The DIS measurements span in the kinematic range from low to high Q^2 , such that the treatment of heavy quarks (charm and beauty) and of their masses becomes important. Several schemes exist and the implemented variants in HERAFitter are briefly discussed as follows.

Zero-Mass Variable Flavour Number (ZM-VFN)[38]:

In this scheme, the heavy quark densities appear in the proton at Q^2 values above $\sim m_h^2$ (heavy quark mass) and the heavy quarks are treated as massless in both the ini- 263 tial and final states. The lowest order process is the scat- 264 tering of lepton off the heavy quark via boson exchange. 265 This scheme is expected to be reliable only in the region 266 with $Q^2 \gg m_h^2$. In HERAFitter this scheme is available 267 for the DIS structure function calculation via interface 268 to the QCDNUM [23] package and it benefits from the fast 269 QCDNUM convolution engine.

Fixed Flavour Number (FFN)[39–41]:

211

214

216

217

218

219

220

227

228

230

233

234

236

239

241

242

243

244

246

247

248

250

251

252

255

257

260

261

262

In this scheme only the gluon and the light quarks are 272 considered as partons within the proton and massive quarks3 are produced perturbatively in the final state. The low- 274 est order process is the heavy quark-antiquark pair pro- 275 duction in the boson-gluon fusion. In HERAFitter this 276 scheme can be accessed via the QCDNUM implementa- 277 tion or through the interface to the open-source code 278 OPENQCDRAD (as implemented by the ABM group) [42]. Through QCDNUM, the calculation of the heavy quark contributions to DIS structure functions are available at Nextto-Leading-Order (NLO), at $O(\alpha_s)$, and only electromagnetic exchange contributions are taken into account. Through the ABM implementation the heavy quark contributions to CC structure functions are available and, for the NC case, the QCD corrections to the coefficient functions at Next-to-Next-to Leading Order (NNLO) are provided at the best currently known approximation [43]. The ABM implementation also includes the running-mass definition of the heavy quark mass [44], which has the advantage of reducing the sensitivity of the DIS cross sections to higher order corrections, and improving the theoretical precision of the mass definition.

General-Mass Variable-Flavour Number (GM-VFN)[45]:

It this scheme, heavy quark production is treated for $Q^2 \le$ m_h^2 in the FFN scheme and for $Q^2 \gg m_h^2$ in a masless scheme. The recent series of PDF groups that use this scheme are MSTW, CT(CTEQ), NNPDF, and HERA-PDF. HERAFitter implements different variants of the GM-VFN scheme and they are presented below:

- GM-VFN Thorne-Roberts scheme: The Thorne-Roberts (TR) scheme [46] was designed to provide a smooth transition from the massive FFN scheme at low scales $Q^2 < m_h^2$ to the massless ZM-VFNS scheme at high scales $Q^2 \gg m_h^2$. However, the original version was technically difficult to implement beyond NLO, and was updated to the TR' scheme [47]. There are two different variants of the TR' schemes: TR' standard (as used in MSTW PDF sets [18, 47]) and TR' optimal [48], with a smoother transition across the heavy quark threshold region. Both variants are accessible within the HERAFitter package at LO, NLO and NNLO.

factorisation schemes that use the renormalization method of Collins-Wilczek-Zee (CWZ) [49]. This scheme unifies the low scale $Q^2 < m_h^2$ and high scale $Q^2 > m_h^2$ regions with a smooth interpolation across the full energy regime. Within the ACOT package, different variants of the ACOT scheme are available: ACOT-Full [50], S-ACOT- χ [51, 52], ACOT-ZM [50], MS at LO and NLO. For the longitudinal structure function higher order calculations are also available. The ACOT-Full implementation takes into account the quark masses and it reduces to ZM MS scheme in the limit of masses going to zero, but it has the disadvantage that it is computationally intensive (addressed in section 4). A compasion of PDFs extracted from the QCD fits to the HERA data with the TR' and ACOT-Full schemes is illustrated in Fig. 4.

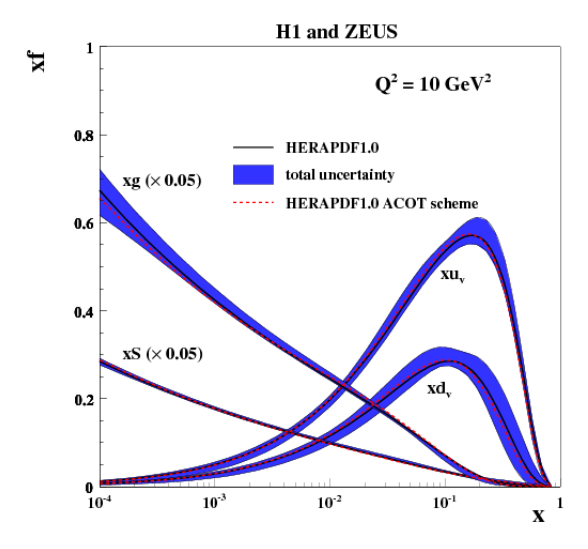


Fig. 4 Overview showing the u- and d-valence, the total sea (scaled), and gluon (scaled) PDFs of the NLO HERAPDF1.0 set [36] with their total uncertainty at the scale of $Q^2 = 10 \text{ GeV}^2$ obtained using the TR' scheme and compared to the PDFs obtained with the ACOT scheme using the k-factor technique (red).

279 3.2 Electroweak Corrections to DIS

280 Calculations of higher-order electroweak corrections to DIS 281 scattering at HERA are available in HERAFitter in the onshell scheme. In this scheme the gauge bosons masses M_W and M_Z are treated symmetrically as basic parameters together with the top, Higgs and fermion masses. These elec-285 troweak corrections are based on the EPRC package [53]. The code provides the running of α using the most recent **GM-VFN ACOT scheme:** The Aivazis-Collins-Olness-parametrisation of the hadronic contribution to Δ_{α} [54], as Tung (ACOT) scheme belongs to the group of VFN well as an older version from Burkhard [55].

3.3 Diffractive PDFs

Similarly to standard DIS, diffractive parton distributions (DPDFs) can be determined from QCD fits to diffractive cross sections. About 10% of deep inelastic interactions at HERA are diffractive, i.e. leading to events in which the interacting proton stays intact $(ep \rightarrow eXp)$. In the diffractive process the proton is well separated from the rest of the hadronic final state by a large rapidity gap. This is interpreted as the dissociation of the virtual photon into hadronic system X with the invariant mass much smaller than W and the same net quantum numbers as the exchanged photon. For such a processes, the diffractive DIS is mediated by the exchange of a hard Pomeron or a secondary Reggeon with the vacuum quantum numbers. The factorisable pomeron picture has proved remarkably successful in the description of most of these data.

The kinematic variables squared four-momentum transfer t (the undetected momentum transfer to the proton system) and the mass M_X of the diffractively produced final state appear for the diffrative process in addition to the usual DIS variables x, Q^2 . In practice, the variable M_X is often replaced by dimensionless quantity $\beta = \frac{Q^2}{M_X^2 + Q^2 - t}$. In models based on a factorisable pomeron, β may be viewed as the fraction of the pomeron longitudinal momentum which is carried by the struck parton, $x = \beta x_{IP}$.

For the inclusive case, the diffractive cross-section reads as:

$$\frac{d\sigma}{d\beta \, dO^2 dx_P \, dt} = \frac{2\pi\alpha^2}{\beta \, O^4} \left(1 + (1 - y)^2 \right) \overline{\sigma}^{D(4)}(\beta, Q^2, x_{IP}, t) \tag{4}$$

with the "reduced cross-section":

310

$$\overline{\sigma}^{D(4)} = F_2^{D(4)} - \frac{y^2}{1 + (1 - y)^2} F_L^{D(4)}.$$
 (5)

Substituting $x = x_{IP}\beta$ we can relate Eq. 4 to the standard DIS formula. In this way, the diffractive structure functions can 339 be employed (see section 4 for details), interfaced to probe expressed as convolutions of the calculable coefficient 340 grams such as MCFM [59-61], available for NLO calculafunctions with the diffractive quark and gluon distribution 341 tions, or FEWZ [62] and DYNNLO [63] for NLO and NNLO. functions, which in general depend on x_{IP} , Q^2 , β , t.

The diffractive PDFs in HERAFitter are implemented following the prescription of ZEUS collaboration [56].

3.4 Drell-Yan processes in pp or $p\bar{p}$ collisions

formation on the different quark densities can be obtained 349 though calculations for higher-order contributions to jet proof the quark sea, in particular to the s density), and associ- 352 68] may be used for the calculation of jet production. Simated W and Z production with heavy quarks (sensitive to s- 353 ilarly to the DY case, the calculation is very demanding in and c-quark densities).

The LO DY triple differential cross section in invariant mass M, boson rapidity y and c.o.m lepton scattering angle $\cos \theta$, for NC, can be written as [57, 58]:

$$\frac{d^3\sigma}{dMdyd\cos\theta} = \frac{\pi\alpha^2}{3MS} \sum_q P_q \left[f_q(x_1, Q^2) f_{\bar{q}}(x_2, Q^2) + (q \leftrightarrow \bar{q}) \right], \tag{6}$$

where *S* is the squared c.o.m beam energy, $x_{1,2} = \frac{M}{\sqrt{S}} \exp(\pm y)$, $f_a(x_1, Q^2)$ is the quark distribution, and P_a is a partonic cross section

The expression for CC scattering has a form:

$$\frac{d^{3}\sigma}{dMdyd\cos\theta} = \frac{\pi\alpha^{2}}{48S\sin^{4}\theta_{W}} \frac{M^{3}(1-\cos\theta)^{2}}{(M^{2}-M_{W}^{2}) + \Gamma_{W}^{2}M_{W}^{2}}$$

$$\sum_{q_{1},q_{2}} V_{q_{1}q_{2}}^{2} f_{q_{1}}(x_{1},Q^{2}) f_{q_{2}}(x_{2},Q^{2}), \tag{7}$$

where $V_{q_1q_2}$ is the Cabibbo-Kabayashi-Masakawa (CKM) quark mixing matrix and M_W and Γ_W are the W boson mass and decay width, respectively.

The simple form of these expressions allows the calcu-326 lation of integrated cross sections without the use of Monte-³²⁷ Carlo (MC) techniques which often introduce statistical fluc-328 tuations. In both NC and CC expressions the PDFs depend only on boson rapidity y and invariant mass M, while the integral in $\cos \theta$ can be solved analytically including the case of realistic kinematic cuts.

Currently, the predictions for DY and W and Z production are available to NNLO and W, Z in association with heavy flavour quarks - to NLO. There are several possibili-335 ties for obtaining the theoretical predictions for DY production in HERAFitter.

The NLO and NNLO calculations are computing power and time consuming and k-factor or fast grid techniques must

3.5 Jet production in ep and pp or $p\bar{p}$ collisions

343 Cross section for production of the high-transverse-momentum hadronic jets is sensitive to the high-x gluon PDF (see e.g. [18]) 345 therefore this process can be used to improve determina-Drell-Yan process provides further valuable information about tion of the gluon PDF, which is particularly important for PDFs. In pp and $p\bar{p}$ scattering, the Z/γ and W production 347 the Higgs production and searches for new physics. Jet proprobe bi-linear combinations of quarks. Complementary in- 348 duction cross sections are currently only known to NLO, alfrom the W asymmetry (d, u and their ratio), the ratio of the 350 duction in proton-proton collisions are now quite advanced [64– W and Z cross sections (sensitive to the flavor composition 351 66]. Within HERAFitter, programs as MCFM or NLOJet++ [67, 354 terms of computing power. Therefore fast grid techniques

section measurements. in ep, pp and $p\bar{p}$ collisions (for de-400 multiplied by the pre-tabulated k-factors. tails see section 4).

3.6 Top-quark production in pp and $p\bar{p}$ collisions

Top-quark pairs $(t\bar{t})$ are produced at hadron colliders dominantly via gg fusion and $q\bar{q}$ annihilation. Measurements of the $t\bar{t}$ cross sections provide additional constraints in particular on the gluon density at medium to high values of x, on $\alpha_{\rm s}$ and on the top-quark mass, m_t [69]. Precise predictions for the total $t\bar{t}$ cross section are available to full NNLO [70]. They can be computed within HERAFitter via an interface to the program HATHOR [71]. Differential $t\bar{t}$ cross section predictions can be used with MCFM [61, 72-75] at NLO accuracy interfaced to HERAFitter with fast grid techniques.

Single top quarks are produced via electroweak interactions and single-top cross sections can be used, for example, to probe the ratio of the u and d densities in the proton as well as the b-quark PDF. Predictions for single-top production are available only at NLO accuracy using MCFM.

4 Computational Techniques

370

more involved with order due to increasing number of Feyn- 425 Instead, it can be assumed that a generic PDF can be apman diagrams. Nowadays even the most advanced pertur- 426 proximated by a set of interpolating functions with a sufbative techniques in combination with modern computing 427 ficient number of strategically well-chosen support points. The direct inclusion of computationally demanding higher- 429 timised in various ways with the simplest one being an incalculation for arbitrary changes in input parameters is not 432 purposes this method can be used to perform the time conscribed as follows.

4.1 k-factor Technique

The k-factors are defined as the ratio of the prediction of a 441 higher-order (slow) pQCD calculation to a lower-order (fast) 442 to facilitate the inclusion of notoriously time consuming jet calculation. Because the k-factors depend on the phase space 443 cross sections at NLO into PDF fits. The APPLGRID [77] probed by the measurement they have to be stored into a 444 package extended first a similar methodology to the DY progrid depending on the relevant kinematic variables. Before 445 duction. While differing in their interpolation and optimisathe start of a fitting procedure the table of k-factors has to 446 tion strategies, both packages construct tables with grids for be computed once for a given PDF with the time consuming 447 each bin of an observable in two steps: In the first step the

are used to facilitate the QCD analyses including jet cross 399 prediction is derived from the fast lower-order calculation

This procedure, however, neglects the fact that the kfactors are process dependent and, as a consequence, they have to be re-evaluated for the newly determined PDF at 404 the end of the fit for the consistency check. Usually, the fit is repeated until input and output k-factors have converged. In summary, this technique avoids iterating the higher-order calculation at each step, but still requires a couple of repetitions depending on the analysis.

- In DIS, appropriate treatments of the heavy quarks require computationally slow calculations. Therefore, "FAST" heavy flavour schemes are implemented in HERAFitter with k-factors defined as the ratio of calculations at the same perturbative order but for massive vs. massless quarks, e.g. NLO (massive)/NLO (massless). These k-factors are calculated only for the starting PDF and hence, the "FAST" heavy flavour schemes should only be used for quick checks, i.e. full heavy flavour schemes are normally recommended. For ACOT case, due to long computation time, the k-factors are used in the default settings in HERAFitter.

420 4.2 Fast Grid Techniques

421 Fast grid techniques exploit the factorisable nature of the Precise measurements require theoretical predictions with 422 cross sections and the fact that iterative PDF fitting proequally good accuracy in order to maximize their impact in 423 cedures do not impose completely arbitrary change in the PDF fits. Perturbative calculations, however, get more and 424 shape of the parameterised functions that represent each PDF. hardware do not lead to sufficiently small turn-around times. 428 The accuracy of this approximation, can be checked and oporder calculations into iterative fits therefore is not possible. 430 crease in the number of support points. Having ensured that Relying on the fact that a full repetition of the perturbative 431 the approximation bias is negligibly small for all practical necessary at each iteration step, two methods have been de- 433 suming higher-order calculations (Eq. 1) only once for the veloped to resolve this problem: the techniques of k-factors 434 set of interpolating functions. Further iteration of a cross and fast grids. Both are available in HERAFitter and de- 435 section evaluation for a particular PDF set is very fast and 436 implies only sums over the set of interpolators multiplied by factors depending on the respective PDF. The approach 438 applies equally for the cross sections of processes involving one or two hadrons in the initial state as well as to their renormalisation and factorisation scale dependence.

This technique was pioneered in the fastNLO project [76] higher-order code. In subsequent iteration steps the theory 448 accessible phase space in the parton momentum fractions x

471

473

476

477

478

480

482

485

487

491

490

500

501

and the renormalisation and factorisation scales μ_R and μ_F 502 is explored in order to optimize the table size. The second 503 step consists of the actual grid construction and filling for the requested observables. Higher-order cross sections can then be restored very efficiently from the pre-produced grids while varying externally provided PDF sets, μ_R and μ_F , or the strong coupling $\alpha_s(O)$. The approach can in principal be extended to arbitrary processes, but requires to establish an interface between the higher-order theory programs and the fast interpolation frameworks. Work in that direction is ongoing for both packages and described in more details in the following:

The fastNLO project [76] has been interfaced to the NLOJet++ program [67] for the calculation of jet production in DIS [78] as well as 2- and 3-jet production in hadron-hadron collisions at NLO [68, 79]. To demonstrate the applicability to higher-orders, threshold corrections at 2-loop order, which approximate the NNLO for the inclusive jet cross section, have been included into the framework as well [80] following Ref. [81]. The latest version of fastNLO [82] allows for a creation of tables where renormalisation and factorisation scales can be varied as a function of two pre-defined observables, e.g. jet transverse momentum p_{\perp} and Q for DIS. The fastNLO code is available online and the jet crosssection grids computed for kinematics of various experiments can be downloaded as well [83].

Dedicated fastNLO libraries and tables required for comparison to particular datasets are included into the HERAFitter
504 5 Fit Methodology package. In this case, the evaluation of the strong coupling constant is taken consistently with the PDF evolution from the QCDNUM code. The interface to the fastNLO tables from within HERAFitter was used in a recent CMS analysis, where the impact on the extraction of the PDFs from the inclusive jet cross section is investigated [15].

In the APPLGRID package [77, 84], in addition to the jet cross sections from NLOJet++ in $pp(\bar{p})$ and DIS pro-The look-up tables (grids) can be generated with the customised versions of the MCFM parton level DY generator [59-61]. The variation of the renormalisation and factorisation scales is possible a posteriori, when calculating theory predictions with the APPLGRID tables, and independent variation of the strong coupling constant is also allowed. For NNLO predictions in HERAFitter kfactors can be also applied within the APPLGRID frame-

The HERAFitter interface to APPLGRID was in particu- 521 5.1 Functional Forms for PDF parametrisation lar used by the ATLAS collaboration to extract the strange ploying the k-factor approach is displayed in Fig. 5 to- $_{524}$ to parametrise PDFs can be used:

gether with the comparison to global PDF sets CT10 [19] and NNPDF2.1 [20].

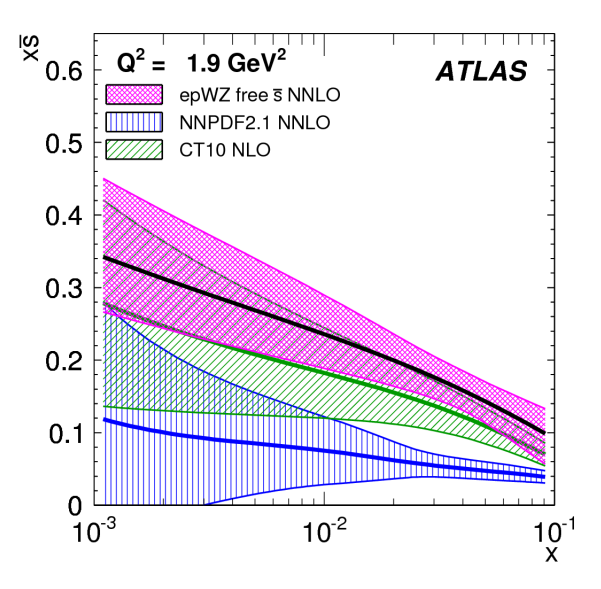


Fig. 5 The strange anti-quark density versus x for the ATLAS epWZ free sbar NNLO fit (magenta band) compared to predictions from NNPDF2.1 (blue hatched) and CT10 (green hatched) at Q^2 1.9 GeV². The ATLAS fit was performed using k-factor approach for NNLO corrections. The figure is taken from [11].

Performing a QCD analysis one usually needs to check stability of the results w.r.t. different assumptions, e.g. the functional parametrisation form, the heavy quarks mass values, ⁵⁰⁸ alternative theoretical calculations, method of minimisation, interpretation of uncertainties, etc. It is also desirable to be able to discriminate or quantify the effect of the chosen ansatz, 511 ideally within a common framework, and HERAFitter is optimally designed for such tests. The methodology employed cesses, the calculations of DY production are implemented. by HERAFitter relies on a flexible and modular framework that allows for independent integration of the state-of-the-art techniques, either related to the inclusion of a new theoretical calculation, or of new approaches to treat uncertainties.

> In this section we briefly describe the available options in HERAFitter. In addition, as an alternative approach to a 519 complete QCD fit, the Bayesian reweighting method, which 520 is also available in HERAFitter, is described.

quark density of the proton from W and Z cross sec- 522 The PDFs are parametrised at a starting scale, chosen to be tions [11]. An illustration of ATLAS PDFs extracted em- 523 below charm mass. In HERAFitter various functional forms

Standard Polynomials: A polynomial form is used to parametrise the *x*-dependence of the PDFs:

$$xf(x) = Ax^{B}(1-x)^{C}P_{i}(x),$$
 (8)

The standard polynomial form is most commonly used by the PDF groups. In HERA PDFs, the parametrised PDFs are the valence distributions xu_v and xd_v , the gluon distribution xg, and the u-type and d-type sea $x\bar{U}$, $x\bar{D}$, where $x\bar{U}=x\bar{u}$, $x\bar{D}=x\bar{d}+x\bar{s}$ at the starting scale. The form of polynomials $P_i(x)$ depdend on the style, defined as a steering parameter. For the HERAPDF [36] style takes the Regge-inspired form $(1+\varepsilon\sqrt{x}+Dx+Ex^2)$ with additional constraints relating to the flavour decomposition of the light sea. For the CTEQ style, $P_i(x)$ takes the form $e^{a_3x}(1+e^{a_4x}+e^{a_5}x^2)$. QCD number and momentum sum-rules are used to determine the normalisations A for the valence and gluon distributions, and the sum-rule integrals are soved analytically.

Bi-Log-Normal Distributions: The parametrisation is motivated by multi-particle statistics and holds the following functional form:

$$xf(x) = ax^{p-b\log(x)}(1-x)^{q-d\log(1-x)}. (9)$$

This function can be regarded as a generalisation of the standard polynomial form described above, however, numerical integration of Eq. 9 is required in order to satisfy the OCD sum rules.

Chebyshev Polynomials: A flexible parameterization employed for the gluon and sea distributions and based on the Chebyshev polynomials. For better modeling the low-x asymptotic of those PDFs, the polynomial of the argument $\log(x)$ are considered. Furthermore, the PDFs are multiplied by the factor of (1-x) to ensure that they vanish as $x \to 1$. The resulting parametric form reads

$$xg(x) = A_g(1-x) \sum_{i=0}^{N_g-1} A_{g_i} T_i \left(-\frac{2\log x - \log x_{\min}}{\log x_{\min}} \right),$$
 (10)

$$xS(x) = (1-x) \sum_{i=0}^{N_S - 1} A_{S_i} T_i \left(-\frac{2\log x - \log x_{\min}}{\log x_{\min}} \right), \tag{11}$$

where T_i are the first-type Chebyshev polynomials of the order i. The normalisation factor A_g is defined from the momentum sum rule which can be evaluated analytically. The values of $N_{g,S}$ up to 15 are allowed, however, already starting from $N_{g,S} \ge 5$ the fit quality is already similar to the standard-polynomial parametrisation with a similar number of parameters.

The low-x uncertainties in the PDFs determined from the HERA data using different parameterizations were studied in [85]. Figure 6 shows the comparison of the gluon density obtained with the parameterization Eq. 10,11 to the standard-polynomial one.

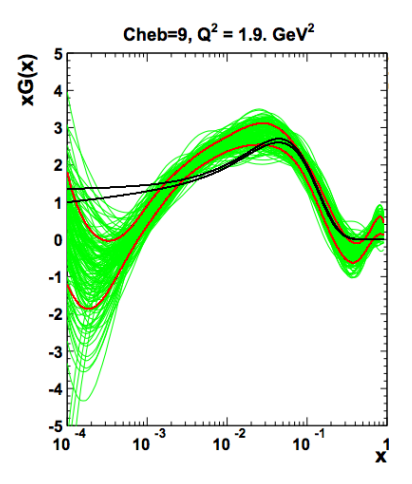


Fig. 6 The gluon density is shown at the starting scale. The black lines correspond to the error band of the gluon distribution using a standard parameterisation and it is to be compared to the case of the Chebyshev parameterisation [85].

External PDFs: HERAFitter provides the possibility to access external PDF sets, which can be used to compute theoretical predictions for the various processes of interest as implemented in HERAFitter. This is possible via an interface to LHAPDF [33, 34] providing access to the global PDF sets available at different orders. HERAFitter also allows to evolve PDFs from LHAPDF using the corresponding grids as an initial evolution boundary condition. Figure 7 illustrates the comparison of the PDFs accessed from LHAPDF as produced with the drawing tools available in HERAFitter.

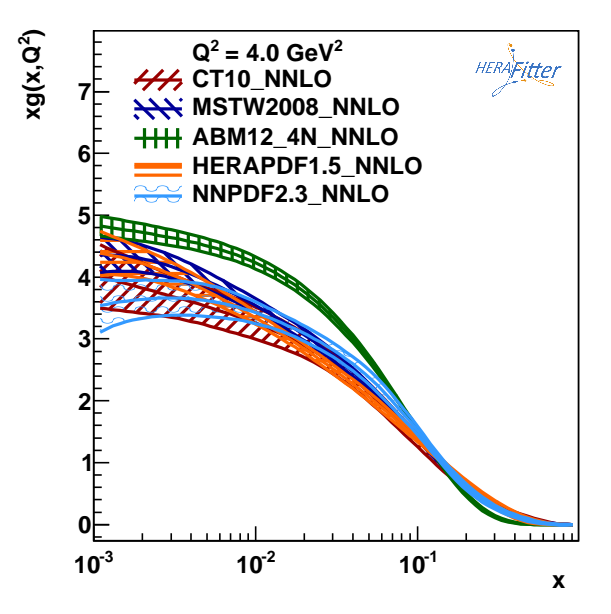


Fig. 7 Gluon density as extracted by various PDF groups at the scale of $Q^2=4~{\rm GeV}^2$, plotted using the drawing tools from HERAFitter.

586

587

590

592

593

594

597

598

600

602

603

604

607

609

611

612

613

614

5.2 Representation of χ^2

The PDF parameters are determined in HERAFitter by minimisation of the χ^2 function taking into account correlated and uncorrelated measurement uncertainties. There are various forms of χ^2 differing by method used to include the experimental uncertainties, e.g. using covariance matrix or providing nuisance parameters to encode dependence of each systematic source for each measurement data point, different 619 Three distinct methods for propagating experimental uncerscaling options, etc. The options available in HERAFitter 620 tainties to PDFs are implemented in HERAFitter and reare following.

Covariance Matrix Representation: For a data point μ_i 622 with a corresponding theory prediction m_i , the χ^2 function can be expressed in the following form:

$$\chi^{2}(m) = \sum_{i,k} (m_{i} - \mu_{i}) C_{ik}^{-1}(m_{k} - \mu_{k}), \tag{12}$$

were the experimental uncertainties are given in a form of covariance matrix $C_{i,k}$ for measurements in bins i an 629 k. The covariance matrix C_{ik} is given by the sum of sta- 630 tistical, uncorrelated and correlated systematic contribu- 631 tions:

$$C_{ik} = C_{ik}^{stat} + C_{ik}^{uncor} + C_{ik}^{sys}. (13)$$

With this representation the particular effect of a certain 635 systematic source of the uncertainty cannot be distin- 636 guished from others.

Nuisance Parameters Representation: For the case when 638 systematic uncertainties are separated by sources the χ^2 form is expressed as

$$\chi^{2}(m,b) = \sum_{i} \frac{\left[\mu_{i} - m_{i} \left(1 - \sum_{j} \gamma_{j}^{i} b_{j}\right)\right]^{2}}{\delta_{i,\text{sunc}}^{2} m_{i}^{2} + \delta_{i,\text{stat}}^{2} \mu_{i} m_{i} \left(1 - \sum_{j} \gamma_{j}^{i} b_{j}\right)} + \sum_{j} b_{j}^{2}, \quad (14)$$

were, μ_i is the central value of the measurement i with 646 its relative statistical $\delta_{i, \mathrm{stat}}$ and relative uncorrelated systematic uncertainty $\delta_{i,\mathrm{unc}}$. Further, γ_i^i quantifies the sensitivity of the measurement to the correlated systematic 649 source j. The function χ^2 depends in addition on the 650 set of systematic nuisance parameters b_j . This defini- 651 tion of the χ^2 function assumes that systematic uncertainties are proportional to the central prediction values 653 (multiplicative errors), whereas the statistical uncertain- 654 ties scale with the square root of the expected number of 655

During the χ^2 minimisation, the nuisance parameters b_i 657 and the PDFs are determined.

Mixed Form Representation: In some cases, the statisti- 659 cal and systematic uncertainties are provided in different 660 forms. For example, the correlated experimental system- 661 atic uncertainties are available as nuisance parameters 662 but the bin-to-bin statistical correlations are given in a 663 form of covariance matrix. HERAFitter offers possibilities to include also the mixed form of treating statistical, uncorrelated and correlated systematic uncertainties.

5.3 Treatment of the Experimental Uncertainties

615

viewed here: the Hessian, Offset, and Monte Carlo method.

Hessian method: The PDF uncertainties reflecting the uncertainties in experimental data are esitimated by examining the shape of χ^2 in the neighborhood of the minimum [86]. Following approach of [86], the Hessian matrix is defined by the second derivatives of χ^2 on the fitted PDF parameters. The matrix is diagonalized and the Hessian eigenvectors are computed. Due to orthogonality, these vectors correspond to statistically independent sources of the uncertainties in the PDFs obtained.

Offset method: The Offset method [87] uses also the χ^2 function for the central fit for which only uncorrelated uncertainties are taken into account. The goodness of the fit can no longer be judged from the χ^2 since correlated uncertainties are ignored. The correlated uncertainties are propagated into the PDF uncertainties performing the variants of fit with the experimental data varied by $\pm 1\sigma$ from the central value for each systematic source. Since the resulting deviation of the PDF parameters from the ones obtained in the central fit are statistically independent, they are combined in quadrature to arive to the total PDF systematic uncertainty.

In most cases, the uncertainties estimated by the offset method are larger than those from the Hessian method.

Monte Carlo method: The Monte-Carlo technique [88, 89] can be used to determine PDF uncertainties. The uncertainties are estimated using the pseudo-data replicas (typically > 100) randomly generated from the measurement central values and their systematic and statistical uncertainties taking into account all point-to-point correlations. The QCD fit is performed for each replica and the PDF central values with their experimental uncertainties are estimated using distribution of the PDF parameters over these fits, i.e. the mean values and standard deviations over the replicas.

The MC method was checked against the standard error estimation of the PDF uncertainties obtained by the Hessian method. A good agreement was found between the methods once the Gaussian distribution of statistic and systematic uncertainties is assumed in the MC approach [32]. This comparison is illustrated in Fig. 8. Similar findings were reported by the MSTW global analysis [90].

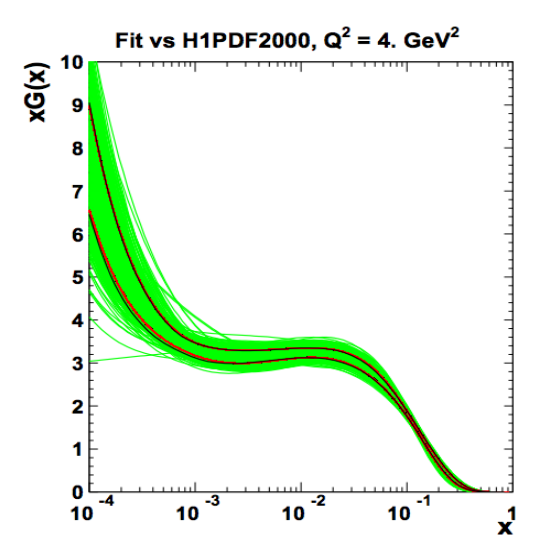


Fig. 8 Comparison between the standard error calculations as employed by the Hessian approach (black lines) and the MC approach (with more than 100 replicas) assuming Gaussian distribution for uncertainty distributions, shown here for each replica (green lines) to- 691 gether with the evaluated standard deviation (red lines) [32]. The black 692 lines in the figure are mostly covered by the red lines.

The nuisance parameter representation of χ^2 in Eq. 14 is 695 derived assuming symmetric experimental errors, however, the published systematic uncertainties are rather often asymmetric. HERAFitter provides the possibility to use asym- 698 metric systematic uncertainties. The implementation relies on the assumption that asymmetric uncertainties can be described by a parabolic function and the nuisance parameter in Eq. 14 is modified as follows

$$m_i(1 - \sum_j \gamma_j^i b_j) \to m_i \left(1 - \sum_j b_j (\boldsymbol{\omega}_j^i b_j + \gamma_j^i)\right),$$
 (15)

where the coefficients ω_j^i , γ_j^i are defined by the up and down values of the systematic uncertainties, S_{ij}^{\pm} ,

$$\omega_{j}^{i} = \frac{1}{2} \left(S_{ij}^{+} + S_{ij}^{-} \right), \qquad \gamma_{j}^{i} = \frac{1}{2} \left(S_{ij}^{+} - S_{ij}^{-} \right).$$
 (16)

The minimisation is performed using fixed number of iterations (typically ten), with rapid convergence.

5.4 Treatment of the Theoretical Input Parameters

The results of a QCD fit depend not only on the input data but also on the input parameters used in the theoretical cal-704 tive PDFs with different choices of the mass of the charm 707 PDF replica: quarks m_c , mass of the bottom quarks m_b and the value of $\alpha_{\rm s}(M_{\rm Z})$, etc. Another important issue is the choice of the functional form for the PDFs at the starting scale and the

value of the starting scale itself. HERAFitter provides possibility of different user choices of various input parameters of the theory.

5.5 Bayesian Reweighting Techniques

As alternative to performing a full QCD fit, HERAFitter allows to assess the impact of including new data in an existing fit using the Bayesian Reweighting technique. Since no fit is performed, the method provides a fast estimate of the impact of new data on PDFs. Bayesian reweighting was first proposed, for the PDF sets delivered in form of Monte Carlo replicas ensembles, in [88] and further developed by the NNPDF Collaboration [91, 92]. More recently, a method to preform Bayesian Reweighting studies starting from PDF fits where uncertainties are provided in form of parameter eigenvectors has been also developed [90]. The latter is based on generating replica set by introducing Gaussian fluctuations on the central PDF set with a variance determined by the PDF uncertainty given by the eigenvectors.

As an alternative to a complete QCD fit, the reweighting method (Bayesian Reweighting) is available in HERAFitter. The method provides a fast estimate of the impact of new data on PDFs. The original suggestion [88] was developed by the NNPDF collaboration [91, 92] and later extended [90] to work not only on the NNPDF replicas, but also on the eigenvectors provided by most PDF groups.

Within the Bayesian Reweighting technique the PDF probability distributions are modified with weights to account for the difference between theory predictions and new data. In the NNPDF method the PDFs are constructed as ensembles of N_{rep} parton distribution functions and observables $\mathcal{O}(PDF)$ are conventionally calculated from the average of the predictions obtained from the ensemble:

$$\langle \mathcal{O}(\text{PDF}) \rangle = \frac{1}{N_{\text{rep}}} \sum_{k=1}^{N_{\text{rep}}} \mathcal{O}(\text{PDF}_k).$$
 (17)

(16) 700 In the case of PDF uncertainties provided by standard Hessian eigenvector error sets, this can be achieved by creating $_{702}$ the k-th random replica by introducing random fluctuations 703 around the central PDF set.

$$w_k = \frac{(\chi_k^2)^{\frac{1}{2}(N_{\text{data}} - 1)} e^{-\frac{1}{2}\chi_k^2}}{\frac{1}{N_{\text{rep}}} \sum_{k=1}^{N_{\text{rep}}} (\chi_k^2)^{\frac{1}{2}(N_{\text{data}} - 1)} e^{-\frac{1}{2}\chi_k^2}},$$
(18)

where $N_{\rm data}$ is the number of new data points, k denotes culations. Nowadays, recent PDF sets address the impact of 705 the specific replica for which the weight is calculated and the choices of theoretical parameters by providing alterna- χ_k^2 is the chi-square of the new data obtained using the k-th

$$\chi^{2}(y, PDF_{k}) = \sum_{i,j=1}^{N_{\text{data}}} (y_{i} - y_{i}(PDF_{k})) \sigma_{ij}^{-1} (y_{j} - y_{j}(PDF_{k})).$$
 (19)

From all the resulting PDF replicas, those providing pre- 748 dictions incompatible with the measurements are discarded. 749 Therefore, reweighted PDFs encompass less replicas than 750 used in the input.

The number of effective replicas of a reweighted sets, 752 that is the size of an equiprobable replicas set containing the 753 same amount of information as the reweighted set in ques-754 tion, is measured by the Shannon Entropy

$$N_{\text{eff}} \equiv \exp\left\{\frac{1}{N_{\text{rep}}} \sum_{k=1}^{N} \text{rep}w_k \ln(N_{\text{rep}}/w_k)\right\}.$$
 (20) ⁷⁵⁷

On the one hand there is no reason in generating a final unweighted set that has a number of replicas (significantly) larger than $N_{\rm eff}$ as no extra information is gained. On the other hand it is advisable to start from a prior PDF set which has as many replicas as possible in order to have a more accurate posterior set at the end of the reweighting procedure.

6 Alternatives to DGLAP formalism

Different approaches that are alternatives to the DGLAP formalism can be used to analyse DIS data in HERAFitter. These include several different dipole models and the use 763 of transverse momentum dependent, or unintegrated PDFs 764 (uPDFs).

6.1 DIPOLE models

737

738

The dipole picture provides an alternative approach to the 769 proton-virtual photon scattering at low x providing the description of both inclusive and diffractive processes. In this 771 approach, the virtual photon fluctuates into a $q\bar{q}$ (or $q\bar{q}g$) dipole which interacts with the proton [93]. The dipoles can 773 be considered as quasi-stable quantum mechanical states, which have very long life time $\propto 1/m_p x$ and a size which is not changed by scattering. The dynamics of the interaction 774 6.2 Transverse Momentum Dependent (Unintegrated) are embedded in the dipole scattering amplitude.

Several dipole models which assume different behavior of the dipole-proton cross sections are implemented in 776 QCD calculations of multiple-scale processes and complex HERAFitter: the Golec-Biernat-Wüsthoff (GBW) dipole sat-777 final-states require in general transverse-momentum depenuration model [28], the colour glass condensate approach 778 dent (TMD) [98], or unintegrated, parton density and parto the high parton density regime called the Iancu-Itakura- 779 ton decay functions [99-107]. The TMD factorisation has Munier (IIM) dipole model [29] and a modified GBW model 780 been proven recently [98] for inclusive DIS. For particular which takes into account the effects of DGLAP evolution 781 hadron-hadron scattering processes, like heavy flavor, vec-

GBW model: In the GBW model the dipole-proton cross section σ_{dip} is given by

$$\sigma_{\text{dip}}(x, r^2) = \sigma_0 \left(1 - \exp\left[-\frac{r^2}{4R_0^2(x)} \right] \right), \tag{21}$$

where r corresponds to the transverse separation between the quark and the antiquark, and R_0^2 is an x-dependent scale parameter which represents the spacing of the gluons in the proton. $R_0^2(x) = (x/x_0)^{\lambda}$ is called the saturation radius. The cross-section normalisation σ_0 , x_0 , and λ are parameters of the model commonly fitted to the DIS data. This model gives exact Bjorken scaling when the dipole size r is small.

IIM model: The IIM model assumes an improved expression for the dipole cross section which is based on the Balitsky-Kovchegov equation [94]. The explicit formula for σ_{dip} can be found in [29]. The alternative scale parameter \tilde{R} , x_0 and λ are fitted parameters of the model.

BGK model: The BGK model is a modification of the GBW model assuming that the spacing R_0 is inverse of the gluon density and taking into account the DGLAP evolution of the latter. The dipole cross section is given

$$\sigma_{\text{dip}}(x, r^2) = \sigma_0 \left(1 - \exp\left[-\frac{\pi^2 r^2 \alpha_s(\mu^2) x g(x, \mu^2)}{3\sigma_0} \right] \right). \quad (22)$$

The factorisation scale $\mu^2 = C_{bgk}/r^2 + \mu_0^2$. The gluon density parametrized at some starting scale Q_0^2 by Eq. 8 is evolved to larger scales using DGLAP evolution. Variables σ_0 , μ_0^2 and three parameters for the gluon density, A_g , λ_g , C_g , are fitted parameters of the model, while C_{bgk} is fixed to 4.0.

BGK model with valence quarks:

767

768

The dipole models are valid in the low-x region only, where the valence quark contribution to the total proton momentum is 5% to 15% for x from 0.0001 to 0.01 [95]. The new HERA F_2 measurements have a precision which is better than 2%. Therefore, in HERAFitter the contribution of the valence quarks can be taken into account in the original BGK model [96, 97].

775 PDFs with CCFM

called the Bartels-Golec-Kowalski (BGK) dipole model [30]. 782 tor boson and Higgs production, TMD factorisation has also been proven in the high-energy (small-x) limit [108–110]

> In the framework of high-energy factorisation [108, 111, 112] the DIS cross section can be written as a convolution in both longitudinal and transverse momenta of the TMD parton density function $\mathcal{A}(x, k_t, \mu)$ with the off-shell partonic

matrix elements, as follows

791

806

808

810

811

812

813

814

815

816

817

819

821

823

824

825

826

$$\sigma_j(x,Q^2) = \int_x^1 dz \int d^2k_t \ \hat{\sigma}_j(x,Q^2,z,k_t) \ \mathscr{A}(z,k_t,\mu)$$
 (23)

with the DIS cross sections σ_i , (j = 2, L) related to the structure functions F_2 and F_L . The hard-scattering kernels $\hat{\sigma}_i$ of Eq. 23, are k_t -dependent and the evolution of the transversemomentum dependent gluon density \mathscr{A} is obtained by combining the resummation of small-x logarithmic contributions [113-115] with medium-x and large-x contributions to parton splitting [6, 9, 10] according to the CCFM evolution equation [26,

The factorisation formula (23) allows resummation of logarithmically enhanced small-x contributions to all orders in perturbation theory, both in the hard scattering coefficients and in the parton evolution, fully taking into account the dependence on the factorisation scale μ and on the factorisation scheme [118, 119].

The cross section σ_i , (j = 2, L) is calculated in a FFN scheme, where only the boson-gluon fusion process ($\gamma^* g^* \rightarrow$ $q\bar{q}$) is included. The masses of the quarks are explicitly included as parameters of the model. In addition to $\gamma^* g^* \to q\bar{q}$, the contribution from valence quarks is included via $\gamma^* q \rightarrow q$ as described later by using a CCFM evolution of valence quarks [120, 121].

CCFM Grid Techniques:

The CCFM evolution cannot be written easily in an ana-

$$x\mathscr{A}(x,k_t,p) = x \int dx' \int dx'' \mathscr{A}_0(x') \mathscr{\tilde{A}}\left(x'',k_t,p\right) \delta(x'x''-x)$$
$$= \int dx' \mathscr{A}_0(x') \cdot \frac{x}{x'} \mathscr{\tilde{A}}\left(\frac{x}{x'},k_t,p\right), \tag{24}$$

agator gluon and p is the evolution variable.

Calculation of the cross section according to Eq. 23 in- 865 lic licence are provided together with the main source code. volves a multidimensional Monte Carlo integration which 866

search for the minimum. Instead the following equation is applied:

$$\sigma(x,Q^2) = \int_x^1 dx_g \mathscr{A}(x_g, k_t, p) \hat{\sigma}(x, x_g, Q^2)$$
$$= \int_x^1 dx' \mathscr{A}_0(x') \cdot \tilde{\sigma}(x/x', Q^2)$$
(25)

Here, first $\tilde{\sigma}(x',Q^2)$ is calculated numerically with a Monte Carlo integration on a grid in x for the values of O^2 used in the fit. Then the last step in Eq. 25 is performed with a fast numerical gauss integration, which can be used in standard fit procedures.

Functional Forms for TMD parameterisation:

For the starting distribution \mathcal{A}_0 , at the starting scale Q_0 , the following form is used:

$$x \mathcal{A}_0(x, k_t) = Nx^{-B} \cdot (1 - x)^C \left(1 - Dx + E\sqrt{x}\right) \exp[-k_t^2/\sigma^2]$$
, (26)

with $\sigma^2 = Q_0^2/2$ and the free parameters N, B, C, D, E. Valence quarks are treated using the method of [120] as described in [121] with a starting distribution taken from any collinear PDF and imposing the flavor sum rule at every scale p.

The TMD parton densities can be plotted either with HERAFitter provided tools or with TMDplotter [35].

7 Applications of HERAFitter

lytic closed form. For this reason a Monte Carlo method 845 HERAFitter is an open source code and it can be downis employed, which is however time-consuming, and can- 846 loaded from [1] together with its supporting documentation. not be used in a straightforward manner in a fit program. 847 A README file is provided within the package together Following the convolution method introduced in [121, 848 with the fast grid theory files (described in section 4) which 122], the kernel $\tilde{\mathscr{A}}(x'', k_t, p)$ is determined from the Monte are associated with the properly formatted data files availabe Carlo solution of the CCFM evolution equation, and then 850 in HERAFitter. The source code contains all the relevant folded with the non-perturbative starting distribution $\mathcal{A}_0(x_0)$, information to perform QCD fits with HERA DIS data as a 852 default set. The performance time depends on the fitting op-853 tions and varies from 10 minutes (using 'FAST' techniques as described in section 4) to several hours when full uncer-(24) 855 tainties are estimated. The HERAFitter code is a combina-856 tion of C++ and Fortran 77 libraries with minimal depenwhere k_t denotes the transverse momentum of the prop- 857 denotes, i.e. for the default fitting options no external de-858 pendences are required except QCDNUM evolution program The kernel \mathcal{A} incorporates all of the dynamics of the 859 [23] and CERN libs. The ROOT libaries are only required for evolution. It is defined on a grid of $50 \otimes 50 \otimes 50$ bins in 800 the drawing tools and when invoking APPLGRID. There are x, k_t, p . The binning in the grid is logarithmic, except for solution also cache options, fast evolution kernels, and usage of the the longitudinal variable x where 40 bins in logarithmic 862 OpenMP (Open Multi-Processing) interface which allows spacing below 0.1, and 10 bins in linear spacing above 863 parallel applications of the GM-VFNS theory predictions in BIS. In addition, the HERAFitter references and GNU pub-

The HERAFitter package was used for the following is time consuming and suffers from numerical fluctua- 867 LHC analyses of SM processes: inclusive Drell-Yan and Wand tions. This cannot be employed directly in a fit procedure 868 Z production [11, 13, 14], inclusive jets [12, 15] production. involving the calculation of numerical derivatives in the 869 The results of QCD analyses using HERAFitter are also

884

published for the inclusive H1 measurements [16] and the 918 recent combination of charm production measurements in 919 DIS [17]. A determination of the transverse momentum dependent gluon density using precision HERA data obtained 921 with HERAFitter has been reported in [123].

The HERAFitter platform has been already used to produce PDF grids from the QCD analyses performed at HERA [36, 124] and at the LHC, using measurements from ATLAS [11, 925 12] (ATLAS PDF sets [125]) which can be used to study predictions for SM or beyond SM processes. Moreover, HERAFitter provides a possibility to perform impact studies for possible 928 future colliders as demonstrated by the QCD studies at the 929 LHeC [126].

Recently a study based on a set of parton distribution 931 functions determined with the HERAFitter program using 932 HERA data was performed [127]. It addresses the issue of 933 correlations between uncertainties for the LO, NLO and NNLO4 sets. These sets are then propagated to study uncertainties 935 for ratios of cross sections calculated at different orders in 936 QCD and a reduction of overall theoretical uncertainty is 937 observed.

8 Summary

The HERAFitter project is a unique platform for QCD analyses to study the structure of the proton. The project successfully encapsulates a wide variety of QCD tools to facilitate investigations of the experimental data and theoretical calculations. HERAFitter is the first open source platform which is optimal for benchmarking studies. It allows for direct comparisons of various theoretical approaches under the same settings, a variety of different methodologies in treating of the experimental and model uncertainties. The growth of HERAFitter benefits from its flexible modular structure driven by QCD advances.

Acknowledgements HERAFitter developers team acknowledges the kind hospitality of DESY and funding by the Helmholtz Alliance "Physic§6 at the Terascale" of the Helmholtz Association. We are grateful to 957 the DESY IT department for their support of the HERAFitter developers. Additional support was received from BMBF-JINR cooperation program, Heisenberg-Landau program, RFBR grant 12-02-91526-CERN a and a dedicated funding of the Initiative and Networking Fond 960 of Helmholtz Association SO-072. We also acknowledge Nathan Hartland with Luigi Del Debbio for contributing to the implementation of 962 the Bayesian Reweighting technique and would like to thank R. Thorne 963 for fruitful discussions.

References

915

916

917

- 1. HERAFitter, https://www.herafitter.org.
- 2. G. Aad *et al.* [ATLAS Collaboration], Phys.Lett. **B716**, 1 (2012), [1207.7214].

- 3. S. Chatrchyan *et al.* [CMS Collaboration], Phys.Lett. **B716**, 30 (2012), [1207.7235].
- 4. E. Perez and E. Rizvi, Rep.Prog.Phys. **76**, 046201 (2013), [1208.1178].
- 5. S. Forte and G. Watt, Ann.Rev.Nucl.Part.Sci. **63**, 291 (2013), [1301.6754].
- 6. V. N. Gribov and L. N. Lipatov, Sov. J. Nucl. Phys. **15**, 438 (1972).
- 7. V. N. Gribov and L. N. Lipatov, Sov. J. Nucl. Phys. **15**, 675 (1972).
- 8. L. N. Lipatov, Sov. J. Nucl. Phys. 20, 94 (1975).
- 9. Y. L. Dokshitzer, Sov. Phys. JETP 46, 641 (1977).
- 10. G. Altarelli and G. Parisi, Nucl. Phys. B **126**, 298 (1977).
- 11. G. Aad *et al.* [ATLAS Collaboration], Phys. Rev. Lett. **109**, 012001 (2012), [arXiv:1203.4051].
- 12. G. Aad *et al.* [ATLAS Collaboration], Eur.Phys.J. **73**, 2509 (2013), [arXiv:1304:4739].
- 13. G. Aad *et al.* [ATLAS Collaboration], Phys. Lett. **B725**, 223 (2013), [arXiv::1305.4192].
- 14. S. Chatrchyan *et al.* [CMS Collaboration], submitted to Phys. Rev. **D** (2014), [arXiv:1312.6283].

939

940

941

942

954

965

967

968

- 15. S. Chatrchyan *et al.* [CMS Collaboration], CMS PAS SMP-12-028 (2014).
- 16. F. Aaron *et al.* [H1 Collaboration], JHEP **1209**, 061 (2012), [arXiv:1206.7007].
- 17. H. Abramowicz *et al.* [H1 and ZEUS Collaborations], Eur. Phys. J. **C73**, 2311 (2013), [arXiv:1211.1182].
- 18. A. Martin, W. Stirling, R. Thorne, and G. Watt, Eur. Phys. J. C 63, 189 (2009), [arXiv:0901.0002], URL http://mstwpdf.hepforge.org/.
- J. Gao, M. Guzzi, J. Huston, H.-L. Lai, Z. Li, et al., Phys.Rev. D89, 033009 (2014), [1302.6246], URL http://hep.pa.msu.edu/cteq/public/.
- R. D. Ball, V. Bertone, S. Carrazza, C. S. Deans, L. Del Debbio, *et al.*, Nucl.Phys. **B867**, 244 (2013), [1207.1303], URL https://nnpdf.hepforge.org/.
- 21. S. Alekhin, J. Blümlein, and S. Moch (2013), [1310.3059].
- 22. P. Jimenez-Delgado and E. Reya, Phys.Rev. **D80**, 114011 (2009), [0909.1711], URL http://www.het.physik.tu-dortmund.de/pdfserver/index.html.
- 23. M. Botje (2010), http://www.nikef.nl/h24/qcdnum/index.html, [arXiv:1005.1481].
- 24. M. Ciafaloni, Nucl. Phys. B 296, 49 (1988).
- 25. S. Catani, F. Fiorani, and G. Marchesini, Phys. Lett. B **234**, 339 (1990).
- S. Catani, F. Fiorani, and G. Marchesini, Nucl. Phys. B 336, 18 (1990).
- 27. G. Marchesini, Nucl. Phys. B 445, 49 (1995).

- 28. K. Golec-Biernat and M. Wüsthoff, Phys. Rev. D **59**, 1023 014017 (1999), [hep-ph/9807513].
- 29. E. Iancu, K. Itakura, and S. Munier, Phys. Lett. **B590**, 1025 199 (2004), [hep-ph/0310338].
- 30. J. Bartels, K. Golec-Biernat, and H. Kowalski, Phys. 1027 Rev. D **66**, 014001 (2002), [hep-ph/0203258].
- 31. F. James and M. Roos, Comput. Phys. Commun. **10**, 1029 343 (1975).
- 32. M. Dittmar, S. Forte, A. Glazov, and S. Moch 1031 (2009), Altarelli, G. and others (contributing authors), 1032 [arXiv:0901.2504].
- 33. M. R. Whalley, D. Bourilkov, and R. Group (2005), 1034 [hep-ph/0508110].

1045

- 34. LHAPDF, URL http://lhapdf.hepforge.org.
- 35. [TMD Collaboration], to be published.

970

97:

974

976

978

979

983

985

988

992

997

1001

1002

1003

1006

1008

1010

1011

1012

1013

1014

1015

1017

1019

1020

102

1022

- 36. F. Aaron *et al.* [H1 and ZEUS Collaborations], JHEP 1038 **1001**, 109 (2010), [arXiv:0911.0884].
- 37. R. Devenish and A. Cooper-Sarkar 1040 (2011), *Deep Inelastic Scattering*, ISBN: 1041 0199602255,9780199602254.
- 38. J. C. Collins and W.-K. Tung, Nucl. Phys. B **278**, 934 1043 (1986).
- 39. E. Laenen *et al.*, Phys. Lett. **B291**, 325 (1992).
- 40. E. Laenen et al., Nucl. Phys. **B392**, 162, 229 (1993).
- 41. S. Riemersma, J. Smith, and van Neerven. W.L., Phys. 1047 Lett. **B347**, 143 (1995), [hep-ph/9411431].
- 42. S. Alekhin, J. Blümlein, and S. Moch, 1049 OPENQCDRAD, description a program and 1050 http://www-1051 code are available via: zeuthen.desy.de/~alekhin/OPENOCDRAD. 1052
- 43. H. Kawamura, N. Lo Presti, S. Moch, and A. Vogt, 1053 Nucl.Phys. **B864**, 399 (2012).
- 44. S. Alekhin and S. Moch, Phys. Lett. **B699**, 345 (2011), 1055 [arXiv:1011.5790].
- 45. R. Demina, S. Keller, M. Kramer, S. Kretzer, R. Mar-1057 tin, *et al.* (1999), [hep-ph/0005112].
- 46. R. S. Thorne and R. G. Roberts, Phys. Rev. D **57**, 6871 1059 (1998), [hep-ph/9709442].
- 47. R. S. Thorne, Phys. Rev. **D73**, 054019 (2006), [hep-1061 ph/0601245].
- 48. R. S. Thorne, Phys. Rev. D **86**, 074017 (2012), 1063 [arXiv:1201.6180].
- 49. J. C. Collins, Phys.Rev. **D58**, 094002 (1998), [hep-1065]
- 50. M. Aivazis, J. C. Collins, F. I. Olness, and W.-K. Tung, 1067 Phys.Rev. **D50**, 3102 (1994), [hep-ph/9312319].
- 51. M. Kramer, F. I. Olness, and D. E. Soper, Phys. Rev. 1069 **D62**, 096007 (2000), [hep-ph/0003035].
- 52. S. Kretzer, H. Lai, F. Olness, and W. Tung, Phys.Rev. 1071 **D69**, 114005 (2004), [hep-ph/0307022].
- 53. H. Spiesberger, Private communication.
- 54. F. Jegerlehner, Proceedings, LC10 Workshop **DESY** 1074 **11-117** (2011).

- H. Burkhard, F. Jegerlehner, G. Penso, and C. Verzegnassi, in CERN Yellow Report on "Polarization at LEP" 1988.
- S. Chekanov *et al.* [ZEUS Collaboration], Nucl. Phys. B831, 1 (2010), [hep-ex/09114119].
- 57. S. D. Drell and T.-M. Yan, Phys. Rev. Lett. **25**, 316 (1970).
- 58. M. Yamada and M. Hayashi, Nuovo Cim. **A70**, 273 (1982).
- J. M. Campbell and R. K. Ellis, Phys. Rev. D60, 113006 (1999), [arXiv:9905386].
- 60. J. M. Campbell and R. K. Ellis, Phys. Rev. **D62**, 114012 (2000), [arXiv:0006304].
- 61. J. M. Campbell and R. K. Ellis, Nucl. Phys. Proc. Suppl. **205-206**, 10 (2010), [arXiv:1007.3492].
- Y. Li and F. Petriello, Phys.Rev. **D86**, 094034 (2012), [arXiv:1208.5967].
- 63. G. Bozzi, J. Rojo, and A. Vicini, Phys.Rev. **D83**, 113008 (2011), [arXiv:1104.2056].
- A. Gehrmann-De Ridder, T. Gehrmann, E. Glover, and J. Pires, Phys. Rev. Lett. 110, 162003 (2013), [arXiv:1301.7310].
- 65. E. Glover and J. Pires, JHEP **1006**, 096 (2010), [arXiv:1003.2824].
- J. Currie, A. Gehrmann-De Ridder, E. Glover, and J. Pires, JHEP **1401**, 110 (2014), [1310.3993].
- 67. Z. Nagy and Z. Trocsanyi, Phys.Rev. **D59**, 014020 (1999), [hep-ph/9806317].
- 68. Z. Nagy, Phys.Rev.Lett. **88**, 122003 (2002), [hep-ph/0110315].
- S. Chatrchyan *et al.* [CMS Collaboration], Phys.Lett. B728, 496 (2014), [1307.1907].
- 70. M. Czakon, P. Fiedler, and A. Mitov, Phys. Rev. Lett. **110**, 252004 (2013), [1303.6254].
- 71. M. Aliev, H. Lacker, U. Langenfeld, S. Moch, P. Uwer, *et al.*, Comput.Phys.Commun. **182**, 1034 (2011), [arXiv:1007.1327].
- J. M. Campbell, R. Frederix, F. Maltoni, and F. Tramontano, Phys.Rev.Lett. 102, 182003 (2009), [0903.0005].
- 73. J. M. Campbell and F. Tramontano, Nucl. Phys. **B726**, 109 (2005), [hep-ph/0506289].
- J. M. Campbell, R. K. Ellis, and F. Tramontano, Phys.Rev. **D70**, 094012 (2004), [hep-ph/0408158].
- 75. J. M. Campbell and R. K. Ellis (2012), report FERMILAB-PUB-12-078-T, [1204.1513].
- 76. T. Kluge, K. Rabbertz, and M. Wobisch, pp. 483–486 (2006), [hep-ph/0609285].
- 77. T. Carli *et al.*, Eur. Phys. J. **C66**, 503 (2010), [arXiv:0911.2985].
- 78. Z. Nagy and Z. Trocsanyi, Phys.Rev.Lett. **87**, 082001 (2001), [hep-ph/0104315].

1079

1081

1083

1084

1085

1088

1090

1092

1093

1097

1099

1104

1106

1108

1109

1116

1118

1119

- ph/0307268].
- 80. M. Wobisch, D. Britzger, T. Kluge, K. Rab-1129 105. F. Hautmann, Acta Phys. Polon. **B40**, 2139 (2009). bertz, and F. Stober [fastNLO Collaboration] (2011), 1130 [arXiv:1109.1310].
- 81. N. Kidonakis and J. Owens, Phys.Rev. **D63**, 054019 1132 (2001), [hep-ph/0007268].
- 82. D. Britzger, K. Rabbertz, F. Stober, and M. Wobisch 1134 108. S. Catani, M. Ciafaloni, and F. Hautmann, Phys. Lett. [fastNLO Collaboration] (2012), [arXiv:1208.3641].
- 83. http://fastnlo.hepforge.org, URL http://fastnlo.1136 hepforge.org.
- 84. http://applgrid.hepforge.org, **URL** http: 1138 //applgrid.hepforge.org.
- 85. A. Glazov, S. Moch, and V. Radescu, Phys. Lett. B 1140 695, 238 (2011), [arXiv:1009.6170]. 1141
- 86. J. Pumplin, D. Stump, R. Brock, D. Casey, J. Hus-1142 ton, et al., Phys.Rev. **D65**, 014013 (2001), [hep-1143] ph/0101032].
- 87. M. Botje, J.Phys. G28, 779 (2002), [hep-ph/0110123]. 1145
- 88. W. T. Giele and S. Keller, Phys.Rev. **D58**, 094023 1146 (1998), [hep-ph/9803393].
- 89. W. T. Giele, S. Keller, and D. Kosower (2001), [hep-1148] ph/0104052]. 1149
- 90. G. Watt and R. Thorne, JHEP 1208, 052 (2012), 1150 116. M. Ciafaloni, Nucl. Phys. B296, 49 (1988). [arXiv:1205.4024].
- 91. R. D. Ball, V. Bertone, F. Cerutti, L. Del Deb-1152 bio, S. Forte, et al., Nucl. Phys. **B855**, 608 (2012), 1153 [arXiv:1108.1758]. 1154
- 92. R. D. Ball et al. [NNPDF Collaboration], Nucl. Phys. 1155 **B849**, 112 (2011), [arXiv:1012.0836]. 1156
- 93. N. N. Nikolaev and B. Zakharov, Z.Phys. C49, 607 1157 (1991).1158
- 94. I. Balitsky, Nucl. Phys. B 463, 99 (1996), [hep-1159 ph/9509348].
- 95. F. Aaron et al. [H1 Collaboration], Eur.Phys.J. C71, 1161 1579 (2011), [1012.4355].
- 96. P. Belov, Doctoral thesis, Universität Hamburg (2013), 1163 [DESY-THESIS-2013-017].
- 97. A. Luszczak and H. Kowalski (2013), [1312.4060].
- 98. J. Collins, Foundations of perturbative QCD, vol. 32 1166 (Cambridge monographs on particle physics, nuclear 1167 physics and cosmology., 2011). 1168
- 99. S. M. Aybat and T. C. Rogers, Phys.Rev. **D83**, 114042 1169 (2011), [1101.5057].
- 100. M. Buffing, P. Mulders, and A. Mukherjee, 1171 Int.J.Mod.Phys.Conf.Ser. 25, 1460003 (2014), 1172 [1309.2472].
- 101. M. Buffing, A. Mukherjee, and P. Mulders, Phys.Rev. 1174 **D88**, 054027 (2013), [1306.5897].
- M. Buffing, A. Mukherjee, and P. Mulders, Phys.Rev. 1124 **D86**, 074030 (2012), [1207.3221]. 1125
 - 103. P. Mulders, Pramana 72, 83 (2009), [0806.1134].

- 79. Z. Nagy, Phys.Rev. **D68**, 094002 (2003), [hep-1127 104. S. Jadach and M. Skrzypek, Acta Phys.Polon. **B40**, 2071 (2009), [0905.1399].

 - 106. F. Hautmann, M. Hentschinski, and H. Jung (2012), [1205.6358].
 - 107. F. Hautmann and H. Jung, Nucl. Phys. Proc. Suppl. 184, 64 (2008), [0712.0568].
 - B 242, 97 (1990).
 - 109. J. C. Collins and R. K. Ellis, Nucl. Phys. B **360**, 3 (1991).
 - 110. F. Hautmann, H. Jung, and V. Pandis, AIP Conf. Proc. **1350**, 263 (2011), [1011.6157].
 - 111. S. Catani, M. Ciafaloni, and F. Hautmann, Nucl. Phys. B 366, 135 (1991).
 - 112. S. Catani, M. Ciafaloni, and F. Hautmann, Phys. Lett. B 307, 147 (1993).
 - 1144 113. L. Lipatov, Phys.Rept. **286**, 131 (1997), [hepph/9610276].
 - 114. V. S. Fadin, E. Kuraev, and L. Lipatov, Phys.Lett. B60, 50 (1975).
 - 115. I. I. Balitsky and L. N. Lipatov, Sov. J. Nucl. Phys. 28, 822 (1978).

 - 117. G. Marchesini, Nucl. Phys. B 445, 49 (1995), [hepph/9412327].
 - 118. S. Catani and F. Hautmann, Nucl. Phys. B 427, 475 (1994), [hep-ph/9405388].
 - 119. S. Catani and F. Hautmann, Phys.Lett. B315, 157 (1993).
 - 120. M. Deak, F. Hautmann, H. Jung, and K. Kutak, Forward-Central Jet Correlations at the Large Hadron Collider (2010), [arXiv:1012.6037].
 - 121. F. Hautmann and H. Jung, Nuclear Physics B 883, 1 (2014), [1312.7875].
 - 122. H. Jung and F. Hautmann (2012), [arXiv:1206.1796].
 - 123. F. Hautmann and H. Jung (2013), [1312.7875].

1160

1165

- 124. HERAPDF1.5LO, NLO and NNLO (H1prelim-13-141 and ZEUS-prel-13-003, H1prelim-10-142 and ZEUSprel-10-018, H1prelim-11-042 and ZEUS-prel-11-002), available via: http://lhapdf.hepforge.org/pdfsets.
- 125. ATLAS **NNLO** epWZ12, available via: http://lhapdf.hepforge.org/pdfsets.
- 1170 126. J. L. Abelleira Fernandez et al. [LHeC Study Group], Journal of Phys. **G**, 075001 (2012), [arXiv:1206.2913].
- 127. HERAFitter Developers Team and M. Lisovyi (2014), [arXiv:1404.4234].